To appear in the *International Journal of Control*
Vol. 00, No. 00, Month 20XX, 1–20

# Iterative Learning Control Applied to a Non-Linear Vortex Panel Model for Improved Aerodynamic Load Performance of Wind Turbines With Smart Rotors

Mark W Blackwell,[a] Owen R Tutty,[a] Eric Rogers[b*] and Richard D Sandberg[a]

[a]Faculty of Engineering and the Environment,
University of Southampton, Southampton SO17 1BJ, UK

[b]Electronics and Computer Science,
University of Southampton, Southampton SO17 1BJ, UK

(*Received 00 Month 20XX; accepted 00 Month 20XX*)

The inclusion of smart devices in wind turbine rotor blades could, in conjunction with collective and individual pitch control, improve the aerodynamic performance of the rotors. This is currently an active area of research with the primary objective of reducing the fatigue loads but mitigating the effects of extreme loads is also of interest. The aerodynamic loads on a wind turbine blade contain periodic and non-periodic components and one approach is to consider the application of iterative learning control algorithms. In this paper the control design is based on a simple, in relative terms, computational fluid dynamics model that uses non-linear wake effects to represent flow past an airfoil. In this paper, a representation for the actuator dynamics is included to undertake a detailed investigation into the level of control possible and on how performance can be effectively measured.

**Keywords:** iterative learning control, wind turbines, flow control

## 1. INTRODUCTION

The aerodynamic forces on wind turbine blades fluctuate and include both deterministic and stochastic elements, where the most obvious stochastic component arises from the variable nature of the wind. This varies in both frequency and magnitude and produces a variation in the aerodynamic load that passes through the turbine system. Deterministic components include the effects of the atmospheric boundary layer, stator-rotor interaction, and yaw misalignment. Both types of disturbance result in loads that require management, especially since blades are relatively flexible structures, and changing blade loads change the blade position relative to the oncoming wind, and hence the aerodynamic loading, thus compounding the complexity of the aero-elastic system.

In basic terms, wind turbine load control involves modifying the lift on the blades and can be achieved by i) varying the blade incidence angle (variable pitch and/or predetermined blade twist), ii) flow velocity (variable rotor speed), iii) blade size (variable blade length), or iv) modifying the blade section aerodynamics (active flow control) (Johnson et al., 2008). This paper considers the last of these and the aim is to damp fluctuations in the lift using circulation control as a model of a blade equipped with a smart rotor.

Smart rotors are currently the subject of research as an advanced control method for large-scale turbines, where supporting literature includes the review paper (Johnson et al., 2008) and

*Corresponding author. Email: etar@ecs.soton.ac.uk

the special issue on this topic (Rice & Verhaegen, 2010), where these rotors would be employed in conjunction with collective and individual pitch control. The goal is to significantly improve aerodynamic performance and load control by integrating smart devices into rotor blades, predominately to reduce fatigue loads but also to attenuate ultimate or extreme loads and regulate power. Aerodynamic devices, for example, trailing edge flaps (Anderson et al., 2010; Lackner & van Kuik, 2010; Castaignet et al., 2013), microtabs (Johnson et al., 2010; Chow & van Dam, 2010), and active vortex generators can be embedded into the blade structure and actively and independently controlled to meet set objectives. Control action of this form offers the potential to increase turbine efficiency and reliability, leading, in turn, to increased blade life and ultimately reduced energy costs (Veers et al., 2003).

Smart rotors can be used across the operational envelope to increase energy capture. At low wind speeds, devices can be activated to improve the aerodynamic performance of the blade, and at high wind speeds, loads can be managed more effectively to ensure performance can be maintained. A reduction in loads would also produce an increase in component lifespan and reduce maintenance. Reducing maintenance costs is especially important given the ongoing trend to operate offshore, where remote environments and difficult access means a dramatic increase in the cost of maintenance operations. This and the increase in rotor blade diameters are major drivers of the need for a step advancement in wind turbine control.

Wind turbines operate in the atmospheric boundary layer where there is a wind shear with a nonuniform mean velocity profile and a regular variation in wind speed past the blade throughout a cycle, even in reasonably steady non-gusting conditions. Hence the flow past the blade will contain an oscillatory component that will be more pronounced toward the tip of the blade, where the greatest speed differential arises.

In a wind farm, a turbine may be downstream of others, which can also add an oscillatory component to the flow. Unsteady flow conditions, relative to the blade, will cause cyclic loads on the blade, in particular, in the lift, and hence, in turn, affect the performance of the turbine. Deterministic disturbances such as repeating oscillations tend to be easier to mitigate against their period and magnitude can be estimated relatively easily from other turbine data, such as rotor speed, diameter, etc. However, there is also a need to reduce the load due to peak or extreme events, particularly those that threaten the structural integrity of the turbine. The objective for control system design should include reducing both the underlying level of disturbance and the peak load. This paper continues to investigate the use of iterative learning control (ILC) in this problem in this area.

The development of ILC was motivated by systems that repeat the same operation over a finite duration with resetting once each execution is complete. An ILC law therefore makes use of previous trial information to update the current trial input to sequentially improve performance from trial-to-trial. The survey papers by Bristow et al. (2006) and Ahn et al. (2007) are a starting point for the ILC literature in which there are designs where a mathematical model of the dynamics is required and others, of a relatively simple structure, where design can be approached in a manner akin to auto-tuning. A (relatively) open research question is to investigate if computational fluid dynamics (CFD) representations can be used for the latter approach, as this would allow the investigation of the effectiveness of relatively simple control structures and, if successful, free up resources in an area where control is very much a necessary but supporting technology. This is a major motivation for the novel work reported in this paper. Other research on ILC for wind turbines, concentrating on its use as an analysis and design tool to determine the control necessary to accurately track reference trajectories during transitions between below and above rated wind conditions, was reported in Laks et al. (2011).

The application of feedback control to smart rotors has been considered in, for example, Lackner & van Kuik (2010) where alleviation of extreme loads using trailing edge flaps was considered and a PID control explicitly designed for fatigue load. This approach gave superior load reduction for small-scale gusts, but not for large-scale global gusts. A frequency-weighted model predictive control was used in Castaignet et al. (2013) with an active 70cm flap on a single blade of a three-bladed

27m diameter turbine. An average 14% reduction of the blade root moment load was obtained, along with a 20% reduction of the amplitude of the load at the frequency of rotation (the 1P load).

Appropriately designed smart rotor control systems offer significant reduction of blade loads by using devices that spanwise distribute load control. Faster active load control is possible as is active feedback based on local measurements. These features supply additional support for ILC and as a starting point, in the interests of ease of implementation, simple structure control laws. This paper uses a CFD model, based on a panel method, to simulate flow past an airfoil. The incoming flow is assumed to be unsteady, but also has added disturbances in the form of vortices that are convected with the flow. Two types of vortices are present in this updated model. Upstream vortices represent non-linear disturbances upstream of the airfoil, while vortices are released from the trailing edge every time step to simulate the Wagner effect of the airfoil wake.

The inclusion of the trailing edge vortices is a significant difference from previous work, which assumed instantaneous lift change (Tutty et al., 2013), and more accurately describes the non-linear flow physics. The vortices interact with each other and with the airfoil, resulting in a nonlinear system. The motion of the vortices is found by solving the Euler equations. Hence, this model introduces both non-periodicity and nonlinearity into the problem in a realistic manner as it is based on a solution to the governing equations for inviscid flow with rotational disturbances convecting in a physically compatible manner.

Devices, such as trailing-edge flaps and microtabs, operate by generating circulation (vorticity) in the region of the trailing edge of the blade, thereby directly affecting the lift on the blade. In the model, the flow at the trailing edge of the airfoil is manipulated to represent these devices and thereby provide the actuation for the control system. Another additional feature of the updated system model is the inclusion of a model of the actuator dynamics. Previous work (Tutty et al., 2013) assumed no delay between the generation of the control input required and the resulting actuation applied to the airfoil. The lift on the airfoil is used as the output of the system and the error between the lift and a fixed target value used to activate the control. Calculating the lift is easily achieved in the numerical model, but in practice would need to be estimated from measurements,for example, form pressure sensors distributed on the surface of the blade.

The ILC literature contains simple structure control laws that can be designed without the requirement of a plant model, i.e., direct from the system input and output. In this paper, phase-lead ILC is combined with a traditional proportional controller. In contrast to other work where a state-space (or equivalent) model is required (e.g., Dong & Verhaegen (2011); Thomsen et al. (2010)), in this paper the CFD model is used to simulate flow past an airfoil. The effectiveness of the control system is assessed with a two-norm measure of the disturbance, which relates to the fatigue load, and an $\infty$-norm, which measures the reduction in the peak disturbance. The airfoil used in this paper is an NREL S825 (Somers, 2005) (Fig. 1). This airfoil is specifically designed for wind turbines, and has a similar profile to the blade sections used in practice.

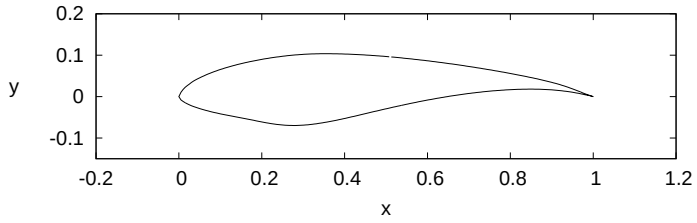


Figure 1. NREL S825 airfoil

This paper starts in the next section with the modeling of the flow, where the model used differs substantially from that used in previous ILC research (Tutty et al., 2013). Next, the ability of the control to suppress the effects of an oscillatory free stream (incoming flow) on the lift of the airfoil is investigated. The following section considers oscillatory flow plus disturbances generated by

convecting vorticity. Then the assumption in previous work (Tutty et al., 2013) of perfect actuator response is replaced by a model of the actuator dynamics. After specifying the actuator model, control scheme performance is evaluated. The final section of the paper gives a critical overview of the results obtained and discusses areas for future research.

## 2. FLOW MODEL

There are two characteristic time scales for flow past a wind turbine blade, i.e., the period of rotation, approximately 5 sec, and typical time for the flow to pass the blade section. The former of these remains relatively constant but the latter varies along the blade, due to both the change in the chord (length) and velocity of the blade section. Moreover, the chord decreases along the blade, e.g., from 4 m near the hub to around 1 m near the tip for a Vestas V112-3.0 MW turbine which has a blade length of 54.6 m. The velocity increases along the blade, giving a significant variation in the characteristic time for the flow to pass the blade.

In this paper the cases of interest are where, using the blade as a reference, disturbances are convected past the blade. Hence the problem is considered in non-dimensional form using the mean free stream velocity $V_\infty$ on a blade section and the chord (length) of the airfoil $H$ as reference values. This is standard aerodynamics and $\mathbf{v}^* = V_\infty \mathbf{v} = V_\infty(v_x, v_y)$ are the velocity components in $\mathbf{x}^* = H\mathbf{x} = H(x, y)$, where the asterisk denotes a dimensional quantity. Time is considered as a non-dimensional quantity using $H/V_\infty$. Hence $t^* = \frac{H}{V_\infty} t$ and the variation of time scales along the blade is now represented by a change in the non-dimensional period of the rotation, increasing with radius. Non-dimensional quantities will be used in the remainder of this paper.

The lift of an airfoil/wing section comes primarily from the pressure exerted by the fluid on the surface of the airfoil. In normal operating conditions, the angle of attack (AoA) is not high enough to provoke separation, hence the flow remains attached, and the pressure distribution on the surface of the blade can be calculated by assuming the flow is inviscid. This greatly simplifies the calculation and is used in this paper but the model employed is substantially different from that in Tutty et al. (2013) due to the inclusion of a wake generated by shedding vorticity in the form of discrete vortices from the trailing edge of the airfoil into the flow. This vorticity then convects downstream as a solution of the Euler equations, the governing equations for inviscid flow. Thus the flow has a representation of the full inviscid dynamics, unlike the simpler model used in Tutty et al. (2013) that assumed a quasi-steady response of the lift generated on the airfoil to changes in the incoming flow.

Relatively simple inviscid models of this kind do exclude extreme cases, such as rapid changes of direction or shear when separation is provoked, but are an acceptable alternative to full Navier-Stokes simulations, which give a complete characterization of the flow, but are too expensive computationally to allow detailed investigation of the control methods. The flow model used in this work allows investigation of feasible control schemes that could eventually be applied to full scale simulations or experiments.

A panel method is used to satisfy the boundary conditions on the surface of the body, where a set of $2N$ discrete panels are used to enforce the boundary conditions at the surface of the body. There are $N$ vortex panels with constant vorticity on each panel ($\lambda_i$), but with the strength varying between the panels. Vortex panels are placed just above the surface of the body and operate by setting the tangential velocity at the surface to zero, from which it follows that, in principle, the kinematic boundary condition of zero normal velocity is satisfied, but only within numerical error, see, for example, Clarke & Tutty (1994) for details. Here the vortex panels are augmented by a similar set of $N$ source panels, of strength $\kappa_i$, placed just below the surface, so that zero normal velocity at the surface is explicitly enforced. For a body with a smooth shape, usually only vortex panels are used as the source panels contribute little ($\kappa_i$ will be small and tend to zero as $N$ increases), but increase the computational effort. However, in this work there is a sharp trailing edge, and a jump in circulation at the trailing edge which is used as actuation. Both of these give

rise to relatively large numerical errors with vortex panels only. Hence source panels are also used to improve the accuracy and the numerical conditioning of the procedure. Details of the vortex and source panels and the velocity fields they generate can be found in many standard texts, such as Anderson (1985).

The source and vortex panels produce a set of $2N$ linear equations in $2N$ unknowns, the $\lambda_i$ and the $\kappa_i$. However, this problem is not well posed and the matrix will be singular (within numerical error). This reflects the fact that there is an infinite set of solutions to the problem of inviscid flow past a body with zero flow across the surface across the body, with the solution varying with the (arbitrary) lift on the body. Here Kelvins circulation theorem is used to provide an extra condition. This states that the total circulation in the flow is constant. Since the circulation is the negative of the integral of the vorticity over the field and the circulation for a vortex panel is $-\kappa_i L_i$ where $L_i$ is the length of panel $i$. The system of equations is now over-determined, with $2N + 1$ equations in $2N$ unknowns. A well-behaved approximate solution is obtained using a least-squares approach, as in Clarke & Tutty (1994), with conservation of circulation/vorticity satisfied exactly.

The base flow consists of the free-stream velocity $\mathbf{V}_0(t) = (V_{0x}(t), 0)$ and the velocity field generated by the vortex panels $\mathbf{v}_p(\mathbf{x}, t) = (v_{px}, v_{py})$, the vortices shed into the wake from the trailing edge, and in addition, disturbances introduced into the flow upstream of the airfoil, also in the form of discrete vortices. The Euler equations governing two-dimensional inviscid incompressible flow can be written in vorticity form as

$$\frac{D\omega}{Dt} \;=\; \frac{\partial\omega}{\partial t} + v_x\frac{\partial\omega}{\partial x} + v_y\frac{\partial\omega}{\partial y} \;=\; 0 \tag{1}$$

where $\omega = \partial v_y/\partial x - \partial v_x/\partial v_y$ is the vorticity, and $D/Dt = \partial/\partial t + v_x\partial/\partial x + v_y\partial/\partial y$ is the material derivative, i.e. the rate of change with time of a material quantity convected with the flow. Moreover, (1) is a statement of the property that in two-dimensional inviscid flow, vorticity is convected with the flow at the local fluid velocity (Batchelor, 1967). Consequently the motion of an individual discrete vortex can be tracked by solving

$$\frac{d\mathbf{x}_v}{dt} \;=\; \mathbf{v}(\mathbf{x}_v, t) \tag{2}$$

where $\mathbf{x}_v$ is the position of the core of the vortex.

The complete velocity field $\mathbf{v}$ is now given by the sum of three components

$$\mathbf{v}(\mathbf{x}, t) \;=\; \mathbf{V}_0 + \mathbf{v}_p + \mathbf{v}_v \tag{3}$$

with

$$\mathbf{v}_v \;=\; \sum_{j=1}^{N_v} \mathbf{v}_{vj} \tag{4}$$

where there are $N_v$ discrete vortices, $\mathbf{v}_{vj}$ denotes the velocity field generated by an individual vortex and given by

$$\mathbf{v}_{vj} \;=\; \Gamma_j \frac{(-(y - y_{vj}), x - x_{vj})}{|\,\mathbf{x} - \mathbf{x}_{vj}\,|^2} F(|\,\mathbf{x} - \mathbf{x}_{vj}\,|) \tag{5}$$

where $\Gamma_j$ is the strength of vortex $j$, $F(s) = \int_0^s \gamma(s)ds$, and $\gamma(s)$ is the vorticity distribution of the core of the vortex. In this work the standard model with a Gaussian distribution is employed, as in Clarke & Tutty (1994). Note that $2\pi \int_0^\infty \gamma(s)ds = 1$ and hence $-\Gamma_j$ is the circulation of the vortex.

The interaction between the discrete vortices and the body produces a nonlinear system of equations for which no closed form solution exists. A numerical solution can be produced by applying any standard time-stepping method to (2) for each of the $N$ discrete vortices, using the velocity at the centre of the vortex from (3). As in Clarke & Tutty (1994), this paper uses a second order Runge-Kutta method to move the vortices

$$\hat{\mathbf{x}}_{vj} = \mathbf{x}_{vj}^k + \frac{1}{2}\Delta t\, \mathbf{v}(\mathbf{x}_{vj}^k, t_k) \tag{6}$$

$$\mathbf{x}_{vj}^{k+1} = \mathbf{x}_{vj}^k + \Delta t\, \mathbf{v}(\hat{\mathbf{x}}_{vj}, t_{k+1/2}) \tag{7}$$

where $t_k = k\Delta t$. At each time step a new vortex is created a distance 1% of the chord length immediately downstream of the trailing edge. For an airfoil without actuation, the strength of the new vortex is given by (see e.g. Cottet & Koumoutsakos (2008))

$$\Gamma_s = -\frac{1}{2}\Delta t(v_a^2 - v_b^2) \tag{8}$$

where $v_a$ and $v_b$ are the magnitudes of the velocity tangential to the surface at the trailing edge, as shown in Fig. 2.

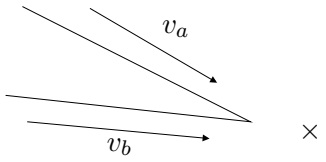


Figure 2. Flow at the trailing edge. The × marks the vortex creation point.

Trailing-edge devices used for lift control act by modifying the flow near the trailing-edge, generating vorticity, which is shed into the wake, and thereby alters the circulation on the body and hence the lift. For example, a trailing edge flap redirects the flow. This can be modeled in a simple manner in the current framework by altering the strength of the new vortex generated at each time step, which will directly change the way the flow leaves the airfoil at the trailing edge, i.e., by assuming the new vortex has strength

$$\Gamma_n = -u \tag{9}$$

when control is applied, where $u$ is the control input of the system, with the lift as output. The lift is calculated in standard fashion from the pressure distribution on the surface of the airfoil (see e.g. Anderson (1985)).

In summary, the model given above is a relatively simple (compared to a full Navier-Stokes simulation) but realistic model of the flow and actuation which can be used to investigate control schemes aimed at damping fluctuations in the lift using trailing-edge devices for load control. The model used here is an alternative to the thin-airfoil type models used in other studies, e.g. by Gaunaa (2010). It is simpler to implement than thin-airfoil type models, with less ad hoc modeling, and is based on a direct solution of the Euler equations, taking explicit account of the thickness of the airfoil. To validate the model, the basic panel code was tested against results from standard sources. In particular, the lift coefficients and pressure distributions for inviscid flow past the airfoil obtained from the method presented above were compared with those found using XFOIL (Drela, 1985), a well validated code commonly used for airfoil calculations. On the basis of the comparison,

398 vortex panels were used. As usual, the panels were clustered towards the trailing-edge, where the curvature is largest.

## 3. OSCILLATORY FLOW

Consider the case with no vortices hence the variation in the lift comes from that in the free stream velocity, and the aim is to damp this fluctuation. The flow past the airfoil, which is at 0° AoA as in Fig. 1, is assumed to be periodic with velocity

$$V_{0x} \;=\; 1 + A\sin(2\pi t/T) \tag{10}$$

where $A$ is the amplitude of the oscillation and $T$ its period (the airfoil rotates one revolution in time $T$, corresponding physically to a rotation time of $HT/V_\infty$). A time step of $\Delta t = 0.005$ is used, with amplitude $A = 0.1$, and a period of $T = 2.5$. A period 10 times greater than previous work (Tutty et al., 2013) is used because it represents a more realistic case without significantly increasing computational efficiency. The initial vorticity on the airfoil is preset to the vorticity expected for the target lift under steady conditions. This is an assumption that the starting vortex has passed far enough downstream to assume the mean bound vorticity on the airfoil is constant and equal to that expected at the target lift. Hence the Wagner effect is not present at the start of the simulations, which is suitable as this work focuses on a wind turbine during continuous operation.

Previous work (Tutty et al., 2013) used a P-type ILC controller as an initial approach to attenuating the periodic disturbance in (10). In this application area, this control scheme is essentially an integral controller and simulates a wake type effect in the model. The present flow model now includes a wake model, therefore using an integral controller again would lead to double counting of the wake effect and the model delivering unreliable results. Consequently a proportional controller is initially used to attenuate the periodic disturbance. At each time step the latest values are used to update the control input,

$$u^k = \mu\,\Delta t\,E^{k-1} \tag{11}$$

where $u^k$ is the control input for step $k$, $\mu$ the gain, and $E^k$ is the error for step $k$ given by

$$E^k = L^k - L_r \tag{12}$$

where $L^k$ is the lift at step $k$ and $L_r$ is the target value for the lift, obtained by taking $A = 0$ in (10). A factor of $\Delta t$ is included in (11) to avoid scaling the gain if a different time step is used (c.f. equation 8).

Figure 3 shows the control input $u^k$ and the error $E^k$ for the controller (11) with $\mu = 10$. Also shown is the error with no control. Improved attenuation is obtained with a larger gain, as shown in Fig. 4. Increasing the gain far enough above 30 eventually causes the scheme to become unstable, although the maximum gain that can be used depends on the problem under consideration, e.g. the maximum gain that can be used with (11) decreases with AoA.

The flow has a forced oscillatory component, the effect of which is only partially damped by the proportional control, as seen in Figures 3 and 4. In previous work (Tutty et al., 2013) a phase-lead ILC was used to damp the oscillation beyond the point achievable by P-type ILC. A similar attempt was made here. The incoming flow and the residual oscillation shown in Figures 3 and 4 operate over cycles of $N_c$ steps where $N_c = T/\Delta t$. Label the cycles as $j$, $j = 0, 1, \ldots$, and the step

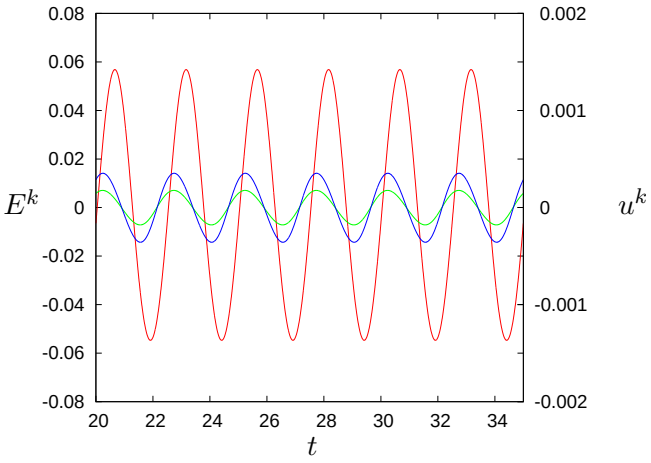


Figure 3. Controller (11) with $\mu = 10$. Error $E^k$ with no control, $u^k = 0$ (red). Error $E^k$ with control (green). Control input $u^k$ (blue).

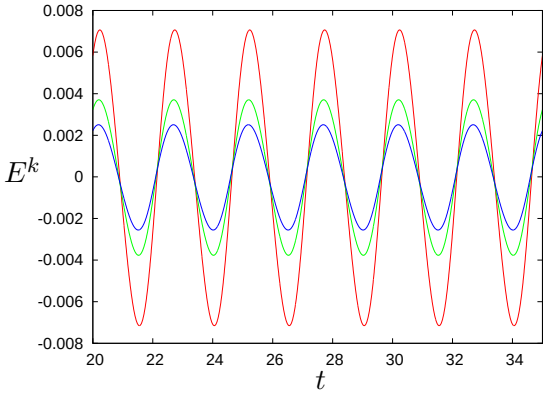


Figure 4. Error $E^k$ for controller (11) with $\mu = 10$ (red), $\mu = 20$ (green) and $\mu = 30$ (blue).

within a cycle as $k_c$, $k_c = 0, 1, \ldots, N_c - 1$, so that $k = jN_c + k_c$. The phase-lead ILC has the form

$$u_j^{k_c} = u_{j-1}^{k_c} + \mu\, \Delta t\, E_{j-1}^{k_c+\Delta} \tag{13}$$

where the shift caused by $\Delta$ is allowed since the complete signal involved is already known (one of the critical features of ILC; such control action has found widespread use in many successful applications as described in the survey papers by Ahn et al. (2007) and Bristow et al. (2006)).

In contrast to the previous work (Tutty et al., 2013), the use of (13) did not successfully damp the error. In Tutty et al. (2013) the flow model with no vortices was linear, and the flow responded directly to the oscillation of the freestream velocity, maintaining a fixed period/frequency. However, in the current work, there is a nonlinear interaction between the action of the control input and the wake formed by the vortices shed into the flow, leading to a change in the dynamics of the flow. In particular, the flow evolves with frequencies which are not harmonics of that of the oscillation of the free stream (10), conflicting with the periodicity assumed in (13). The result is that although there may be some initial damping of the fluctuation in the lift, at longer times the control action provokes disturbances which generate larger fluctuations than those found with the uncontrolled flow. This is illustrated in Figure 5, which shows the control input and error for (13) with $\mu = 1$ and $\Delta = 0$. The calculation was continued past the time shown in Figure 5, with increasing large amplitude fluctuations in both the error and control input, until the simulation failed completely. Similar behaviour was found with other values of the gain. In general, a larger gain provoked large

scale, non-periodic, fluctuations in a shorter time, while, with smaller values, the process took longer but with a similar end result.

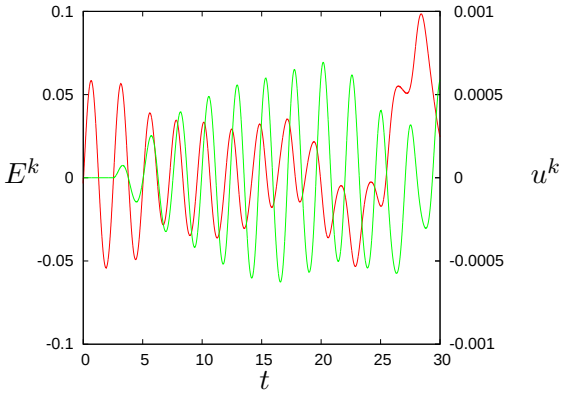


Figure 5. Controller (13) with $\mu = 1$ and $\Delta = 0$. Error $E^k$ (red) and control input $u^k$ (green).

Although the P-type ILC leaves a residual oscillation and the phase-lead ILC fails, a combination of both with suitable gains rapidly damps the fluctuation in the lift to an arbitrarily smaller value. Specifically, we use

$$\hat{u}_j^{k_c} = u_{j-1}^{k_c} + \mu_0 \, \Delta t \, E_{j-1}^{k_c+\Delta} \tag{14}$$

$$\bar{u}^k \;=\; \mu_1 \, \Delta t \, E^{k-1} \tag{15}$$

and

$$u_j^{k_c} \;=\; \hat{u}_j^{k_c} + \bar{u}^k \tag{16}$$

The error $E^k$ and control input $u^k$ for the two-term controller (14-16) with $\mu_0 = 1$, $\mu_1 = 30$ and $\Delta = 0$ are shown in Figure 6. The fluctuations in the lift are rapidly damped, with the control input taking an oscillatory form, with the same period as the fluctuations in the free stream velocity. Different combinations of gains were investigated with the expected results; larger gains gave faster attenuation of the error, provided they were not so large as to provoke instability, with the maximum gains that could be used depending on the specifics of the problem, e.g. the AoA of the airfoil. The gains used for Figure 6 ($\mu_0 = 1,\ \mu_1 = 30$) are used for all results presented below as these produced a suitable combination of attenuation of the error and robustness to changes in the problem definition.

It has been shown in previous work (Tutty et al., 2013) that, for a linear aerodynamic model, the system becomes unstable for all conditions where $\Delta \neq 0$. As the aerodynamic model is now fully non-linear, it is no longer possible to perform a similar stability analysis. However, in practice a much greater level of robustness to varying values of $\Delta$ is observed when the wake is accounted for in the flow model. For the case shown above in Figure 6, values of $\Delta$ up to $\pm 200$ (two fifths of a cycle) were tested. In all cases stability was maintained. For values of $\Delta$ from up to 100 there was little effect of the performance of the controller for non-zero positive $\Delta$, but a degradation of performance (larger errors) during the initial phase of the simulation while the input signal was developing for $\Delta > 100$. For $\Delta < 0$ there was a gradual loss of performance as the magnitude of $\Delta$ was increased in the initial stages of the simulations. However, in all cases the error was damped to a small level ($E^k = O(10^{-6})$) if the simulation was run long enough ($t$ approximately 30 or greater). All results presented below involving the phase-lead ILC have $\Delta = 0$.

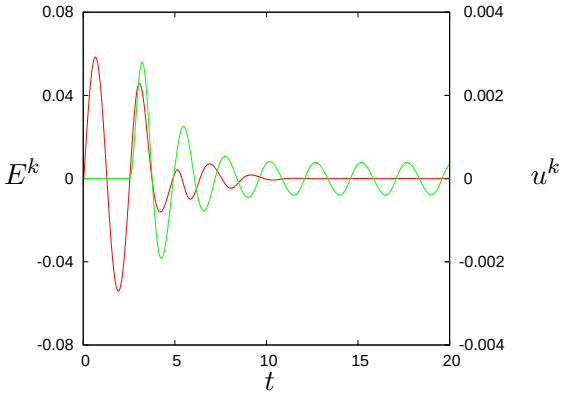


Figure 6. Controller (14-16) with $\mu_0 = 1$, $\mu_1 = 30$ and $\Delta = 0$. Error $E^k$ (red) and control input $30 \times u^k$ (green).

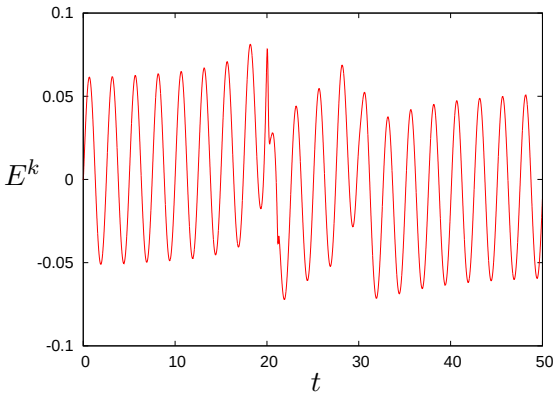


Figure 7. Error $E^k$ for oscillatory flow past the airfoil with two vortices with no control (case 1).

## 4. FLOW WITH VORTICAL DISTURBANCES

In this section, vortices are introduced into the flow and hence it is no longer periodic although it still has a periodic component from the free stream. The addition of the vortices adds another non-linear effect to the system.

Consider the flow with an oscillatory free stream with $A = 0.1$ and $T = 2.5$, as above, and with two vortices introduced into the flow upstream of the airfoil, one with strength $\Gamma_1 = \frac{1}{10}$ placed at $\mathbf{x}_{v1} = (-30, 0.25)$ and the other also with strength $\Gamma_2 = \frac{1}{10}$ but at $\mathbf{x}_{v2} = (-20, -0.35)$ at the start of the simulation ($t = 0$). With these starting values, vortex 1 will pass above the airfoil and vortex 2 below it, generating a significant disturbance in the lift in addition to that from the oscillation in the free stream velocity. Figure 7 shows the error for this flow with no control for the time that the vortices are passing the airfoil (approximately $t = 20$ and $t = 30$). In addition to the oscillation in lift arising from the free stream, large disturbances are generated by the vortices.

The P-type controller (11) with $\mu = 30$ and a target value of the lift for undisturbed flow ($L_r = 0.379$) was applied to this flow. This suppressed most of the effect the disturbance due to the vortices but, as before, left a residual oscillation, as can be seen in Figure 8. Again, this residual oscillation can be largely suppressed by applying the two-term controller incorporating both proportional and phase-lead ILC (14-16) (Figure 9). With the two-term controller, the oscillatory component of the fluctuation has been almost completely eliminated, while the disturbance from the vortices has been heavily damped. The control input $u^k$, shown in Fig. 10, tracks the lift for the uncontrolled flow although with a phase difference (due to the Wagner effect), generating a counterbalancing force to the inherent fluctuation in the lift.

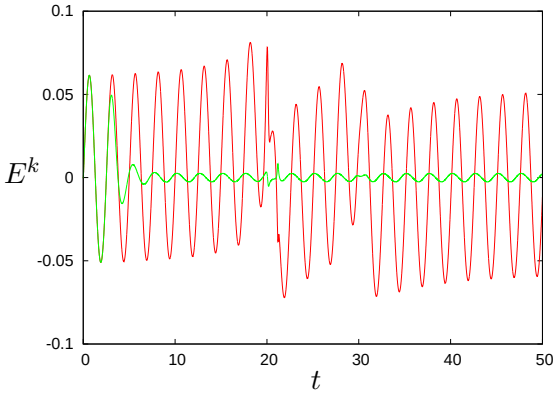


Figure 8. No control error $E^k$ for case 1 (red). Error $E^k$ for controller (11) with $\mu = 30$ (green).

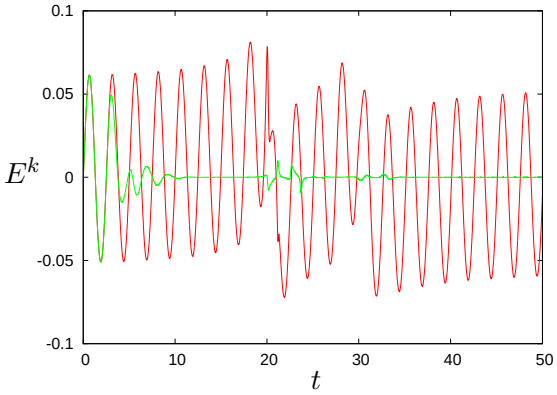


Figure 9. No control error $E^k$ for case 1 (red). Error $E^k$ for controller (14-16) with $\mu_1 = 30$ (green), $\mu_0 = 1$ and $\Delta = 0$ (green).

Table 1. Parameters for selected cases using the two term ILC.

| case | $M$ | AoA | $A$ | $T$ | $L_r$ | $T_0$ | $T_1$ |
|---|---|---|---|---|---|---|---|
| 1 | 2 | 0° | 0.1 | 2.5 | 0.379 | 10 | 50 |
| 2 | 2 | 7° | 0.1 | 2.5 | 0.802 | 10 | 50 |
| 3 | 2 | 7° | 0.1 | 2.5 | 0.802 | 10 | 50 |
| 4 | 2 | 0° | 0.1 | 10 | 0.379 | 50 | 250 |
| 5 | 2 | 7° | 0.1 | 10 | 0.802 | 50 | 250 |
| 6 | 12 | 0° | 0.05 | 20 | 0.379 | 100 | 250 |

A large number of different configurations (number, starting positions and strengths of vortices; AoA, period and amplitude of oscillation of the flow) were investigated, and it was found that using $\mu_0 = 30$ and $\mu_1 = 1$ gave a suitable combination of attenuation of the fluctuation in the load while maintaining stability under widely varying conditions. The two-term control showed a similar tolerance to non-zero values of $\Delta$ as discussed above for the two-term ILC with purely oscillatory flow.

Calculations have been performed using the two-term ILC with $\mu_0 = 30$, $\mu_1 = 1$ and $\Delta = 0$ for a variety of parameter settings and representative results are now discussed. The basic parameters are listed in Table 1, where $M$ is the number of vortices placed upstream of the airfoil at the start of the simulation. Below, in this section, Figs. 8-10 are for case 1, Fig. 11 is for case 4, and Figs. 12 and 13 are for case 6.

Two measures have been used to estimate the degree of damping, a 2-norm with

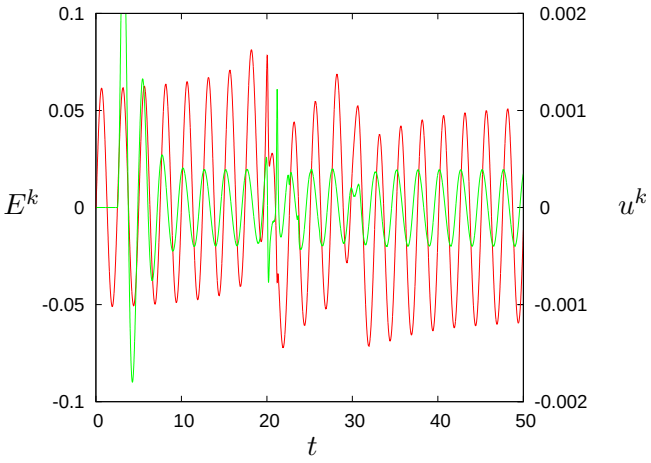


Figure 10. No control error $E^k$ for case 1 (red). Control input $u^k$ for controller (14)-(16) with $\mu_0 = 30$, $\mu_1 = 1$ and $\Delta$ applied to case 1 (green).

Table 2. Error norms for selected cases using the two term ILC.

| case | norm | no control | control | ratio×100 |
|---|---|---|---|---|
| 1 | $\mathcal{L}_2$ | 0.0411 | 0.0013 | 3.1 |
| | $\mathcal{L}_\infty$ | 0.0812 | 0.0100 | 12.3 |
| 2 | $\mathcal{L}_2$ | 0.0843 | $7.5 \times 10^{-4}$ | 0.9 |
| | $\mathcal{L}_\infty$ | 0.1469 | 0.0045 | 3.1 |
| 3 | $\mathcal{L}_2$ | 0.0923 | 0.0020 | 2.2 |
| | $\mathcal{L}_\infty$ | 0.2324 | 0.0135 | 5.8 |
| 4 | $\mathcal{L}_2$ | 0.0444 | $5.6 \times 10^{-5}$ | 0.1 |
| | $\mathcal{L}_\infty$ | 0.0916 | $4.5 \times 10^{-4}$ | 0.5 |
| 5 | $\mathcal{L}_2$ | 0.0900 | $3.4 \times 10^{-5}$ | 0.04 |
| | $\mathcal{L}_\infty$ | 0.1608 | $1.9 \times 10^{-4}$ | 0.1 |
| 6 | $\mathcal{L}_2$ | 0.0235 | $1.4 \times 10^{-4}$ | 0.6 |
| | $\mathcal{L}_\infty$ | 0.0406 | 0.0013 | 3.2 |

$$\mathcal{L}_2 = \left[ \frac{1}{T_1 - T_0} \int_{T_0}^{T_1} (L(t) - L_r)^2 dt \right]^{\frac{1}{2}} \tag{17}$$

and an $\infty$-norm with

$$\mathcal{L}_\infty = \max_k \mid L^k - L_r \mid \tag{18}$$

In general terms, $\mathcal{L}_2$ can be interpreted as measuring the fatigue load and $\mathcal{L}_\infty$ the peak load on the blade. If the mean value of the lift was the target value $L_r$, then $\mathcal{L}_2$ would give the standard deviation of the lift. In all the cases listed in Table 1, the mean value of the lift is close to the target value and hence that the standard deviation of the lift is close to the $\mathcal{L}_2$ value. Also, the range of values for the lift lies within the $L_r$ plus or minus the value of $\mathcal{L}_\infty$. The integration for $\mathcal{L}_2$ was performed over the time the vortices pass the airfoil, with an initial value ($T_0$) that allows the controller to settle (approximately $5T$). Table 2 gives values of the norms for various cases listed in Table 1. This table also gives the ratio of the measures for controlled versus uncontrolled flow. For the case considered above (case 1), the two term ILC produces a reduction of around two orders of magnitude in $\mathcal{L}_2$ and one in $\mathcal{L}_\infty$. Proportionally, these were the smallest reductions in error for any of the cases listed in Table 1 (Table 2).

The airfoil shown in Fig. 1 is at zero degrees angle of attack (AoA). Pitch control (adjusting the AoA) can be used to maintain a near constant loading on the turbine as the mean flow rate varies. For 7° AoA, with the same flow parameters as above and two vortices starting in the same positions as above (case 2: Table 1), the values of the $\mathcal{L}_2$ and $\mathcal{L}_\infty$ ratios are less than a third of the magnitude of the 0° AoA case (case 1). In this case the target value was $L_r = 0.802$, the lift for unperturbed flow with $V_{0x} = 1$ and 7° AoA.

A more extreme case is obtained by changing the strength of vortex 2 to $\Gamma_2 = -\frac{3}{10}$ (case 3). As this vortex contains (in magnitude) over a third of the circulation of that bound to the airfoil in the reference condition, this case can be regarded as a severe test of the control scheme. There is now a larger deviation from the reference value of the lift, as shown in the larger value of $\mathcal{L}_\infty$ (Table 2), but, again, given the extreme nature of this test, the control performs well. However, both $\mathcal{L}_2$ and $\mathcal{L}_\infty$, the values with the control relative to those for the uncontrolled case (Table 2), are larger than for the original two vortex case (i.e. that with $\Gamma_2 = \frac{1}{10}$; case 2).

As mentioned above, both the chord length $H$ and the reference velocity $V_\infty$ will vary along a turbine blade, which implies an increase in the non-dimensional period of the oscillation $T$, moving towards the tip (as $t^* = \frac{H}{V_\infty}t$). All the calculations so far have used $T = 2.5$, which represents flow near the base of the blade. This enabled the interaction between the forced oscillation, the convective disturbance represented by the vortices and the control scheme to be investigated with a relatively small computational effort. In practice, over much of the blade $T$ would be much larger. Figure 11 shows the error for a run with two vortices (as for Figs. 7-10), no control, 0° AoA and $T = 10$ over the time that the vortices pass the airfoil (case 4). The vortices now start much further upstream, at $(-125, 0.25)$ and $(-119, 0.25)$, with strengths $\Gamma_1 = 0.1$ and $\Gamma_2 = -0.1$. Again there is a relatively large fluctuation as the vortices pass. Figure 11 shows the error for the two-term ILC controlled case with $\mu_0 = 30$ and $\mu_1 = 1$. The disturbances are almost completely attenuated (Figure 11 also shows $100E^k$ to better illustrate the effect of the effect of the vortices when the control is active)). There is a two to three order of magnitude reduction in $\mathcal{L}_2$ and $\mathcal{L}_\infty$ (case 4, Table 2). Figure 11 also shows the control input for this case. Again, it tracks the error but with a phase difference due to the non-linear response of the wake to the shed vorticity, which can also be seen in Figures 3, 5, 6 and 10 above. The airfoil was then pitched to 7° AoA and the control works very well with a three order of magnitude reduction in the errors (case 5, Table 2).

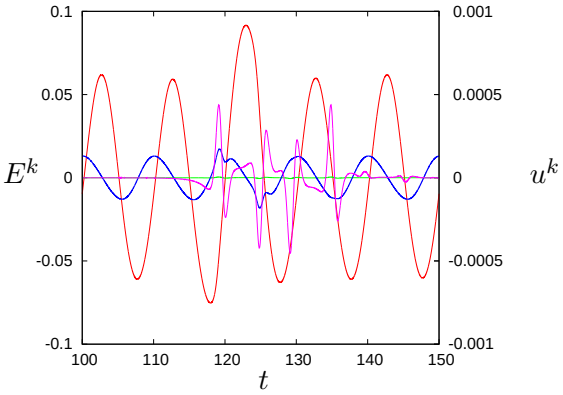


Figure 11. No control error $E^k$ for case 4 (red). Error $E^k$ for controller (14)-(16) with $\mu_0 = 30$, $\mu_1 = 1$ and $\Delta = 0$ (green) (error scaled by 100, magenta), and control input $u^k$ (blue).

For all the results presented above, only a few strong vortices have been used, generating large disturbances in the flow. Figure 12 shows the fluctuation in the lift for a run with 12 relatively weak vortices ($\Gamma_j = \pm 0.01$) as the vortices pass the airfoil when there is no actuation ($u^k = 0$), a period of $T = 20$ and a 5% amplitude in the free stream velocity oscillation ($A = 0.05$). In this case, the vortices generate relatively weak changes in the lift, superimposed on the oscillation from the unsteady nature of the free stream. Figure 12 also shows the error in the lift with the two-term

ILC. Again there is a two order of magnitude reduction in $\mathcal{L}_2$ and $\mathcal{L}_\infty$ (case 6, Table 2). The control signal $u^k$ for this case was similar in form to other cases discussed above, i.e. essentially oscillatory but with relatively short-scale fluctuations generated by the vortices, as shown in Figure 13.

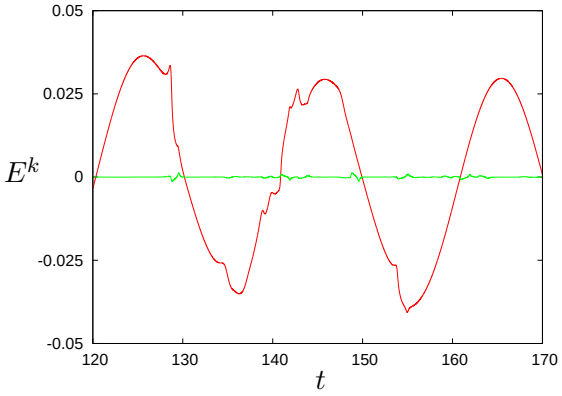


Figure 12. No control error $E^k$ for case 6 (red). Error $E^k$ for controller (14)-(16) with $\mu_0 = 30$, $\mu_1 = 1$ and $\Delta = 0$ applied to case 6 (green).

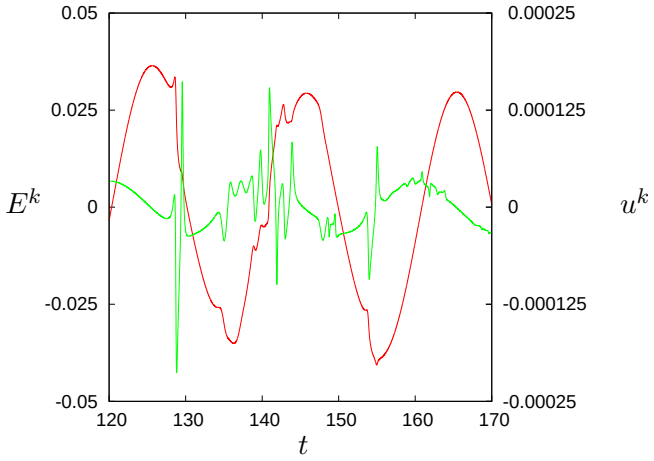


Figure 13. No control error $E^k$ for case 6 (red). Control input $u^k$ for controller (14)-(16) with $\mu_0 = 30$, $\mu_1 = 1$ and $\Delta = 0$ applied to case 6 (green).

In addition to the six cases listed in Table 1, well over a 100 other runs were performed, with different amplitudes and periods of oscillations, numbers and strengths of vortices, at 0°, 7° and 10° AoA. The values given in Table 2 are representative.

## 5. ACTUATOR DYNAMICS

Work in the previous sections has assumed an instantaneous response from the modeled actuator. This is not realistic behaviour for a physical smart rotor system and in application there will be a delay between the controller calculating the control input and the actuator producing the circulation change required. To model this, we assume

$$\frac{du}{dt} = \lambda(\hat{u} - u) \tag{19}$$

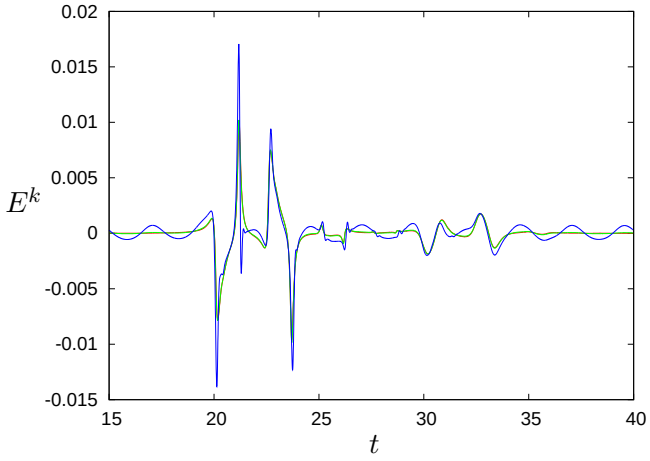


Figure 14. Error $E^k$ for controller (14)-(16) with $\mu_0 = 30$, $\mu_1 = 1$ and $\Delta =$ applied to case 1 with no delay (red), $\lambda = 100$ and $\lambda = 10$ (blue). The errors for no delay and with $\lambda = 100$ are almost the same when plotted at this level.

where $u$ is the actual control input, $\hat{u}$ the input as calculated above from the two-term ILC (14-16), and $\lambda$ is a constant which determines the speed of the response. With a constant input $\hat{u}$, we get a standard first order lag with an exponential behaviour in $u$. A measure of the actuator response is given by the time it takes $u$ to reach 90% of $\hat{u}$ when $\hat{u}$ is constant. In non-dimensional terms this is $2.3/\lambda$. Increasing the value of $\lambda$ will result in a quicker actuator response.

Figure 14 shows the error for the two term ILC controller ($\mu_0 = 30$, $\mu_1 = 1$ and $\Delta = 0$) when applied to the disturbance in case 1 ($T = 2.5$, 2 vortices, 0° AoA) with $\lambda = 10$ and 100 for the time during which the vortices past the airfoil. It also shows the base case with no delay, which, at the level shown, is virtually the same as that with no delay. The results illustrate that the value of $\lambda = 100$ produces an attenuation very close to that of the instantaneous controller. Although $\lambda = 10$ results in poorer performance as the effects of the vortices and periodic disturbance in the flow become more pronounced in the error response. However, the fluctuations are still damped significantly, with the remaining oscillation an order of magnitude less than that with no control, as seen in Figures 10 and 14. Reducing the value of $\lambda$ further reduces the level of attenuation and results in an error signal similar to the uncontrolled flow, as shown in Fig. 15; in particular, the error with $\lambda = 0.1$ and 0.01 are similar in magnitude to that for uncontrolled flow. This is an indication that the level of actuator delay is a limiting factor in achieving the desired attenuation.

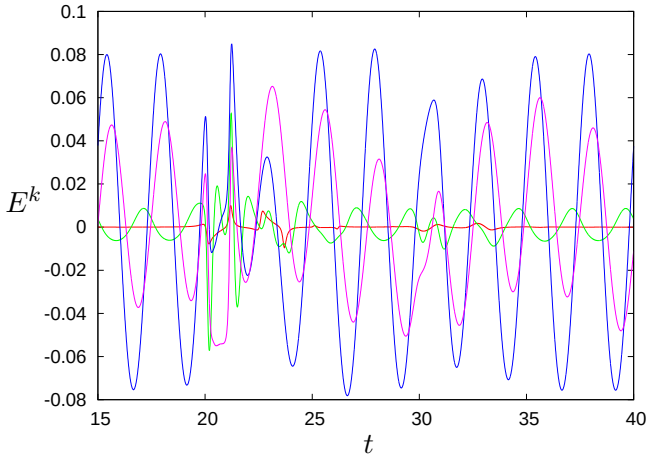


Figure 15. Error $E^k$ for controller (14)-(16) with $\mu_0 = 30$, $\mu_1 = 1$ and $\Delta = 0$ applied to case 1 with no delay (red), $\lambda = 1$ (green), $\lambda = 0.1$ (blue) and $\lambda = 0.01$ (magenta).

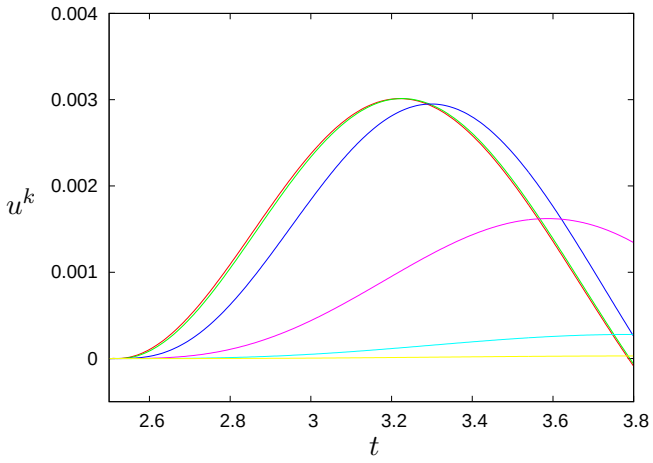


Figure 16. Control inputs $u^k$ for the actuator delays $\lambda$ in Figures 14 and 15. No delay (red), $\lambda = 100$ (green), $\lambda = 10$ (blue), $\lambda = 1$ (magenta), $\lambda = 0.1$ (light blue), $\lambda = 0.01$ (yellow).

Figure 16 illustrates the different control input responses for the $\lambda$ values in Figs. 14 and 15. The controller is activated after one full period has elapsed (at $t = 2.5$ in this case). As expected, increasing the value of $\lambda$ results in a faster control response with $\lambda = 100$ producing an almost identical control input to the idealized instantaneous actuator. Decreasing values of $\lambda$ results in a much slower response, hence the reduced levels of attenuation for smaller values of $\lambda$. Figure 17 illustrates the ratio x 100 for $\mathcal{L}_2$ and $\mathcal{L}_\infty$ norms for cases 1, 2 and 3 ($T = 2.5$, Table 1) with different values of $\lambda$ using the two term ILC controller ($\mu_0 = 30$, $\mu_1 = 1$ and $\Delta = 0$). The figure illustrates a common pattern across these cases in that $\lambda \leq 0.1$ gives, in general, no significant attenuation. In contrast, $\lambda \geq 10$ does give significant attenuation in both measures for all three cases. For $\lambda = 1$, there is attenuation of the oscillatory component as measured by the $\mathcal{L}_2$ norm, but a much weaker effect on the peak values ($\mathcal{L}_\infty$. This behaviour can also been seen in the Figure 15. For $\lambda = 100$, the values of both measures are close to those for the case with instantaneous actuation (less than 1% different in $\mathcal{L}_2$, approximately 2% in $\mathcal{L}_\infty$). $\lambda = 10$ produces larger values that those for the instantaneous actuation, but the worst case ($\mathcal{L}_\infty$ for case 1) still shows an 80% reduction the norm, i.e. the peak value of the error. The fact that the control does produces a moderate drop in the $\mathcal{L}_2$ norm for $\lambda = 0.01$ but an increase for $\lambda = 0.1$ is due to the delay in the actuation introducing a change in phase of the actuation relative to the oscillation in the free steam velocity; this is discussed below.

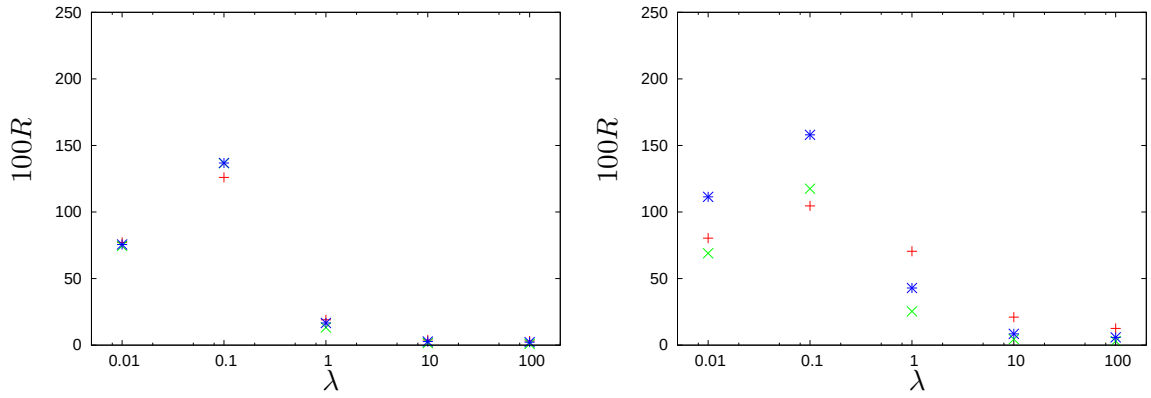


Figure 17. Error norms for controller (14-16) with $\mu_0 = 30$, $\mu_1 = 1$ and $\Delta = 0$ for different $\lambda$; left, $\mathcal{L}_2$ and right, $\mathcal{L}_\infty$. Case 1 (red), case 2 (green) and case 3 (blue). $R$ is the ratio of the norms against the values for no delay.

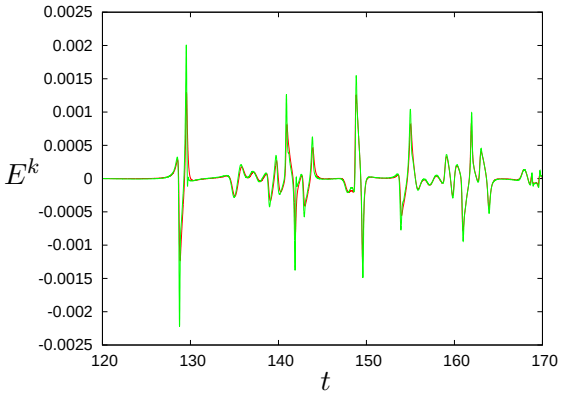


Figure 18. Error $E^k$ for controller (14)-(16) with $\mu_0 = 30$, $\mu_1 = 1$ and $\Delta = 0$ applied to case 6 with no delay (red) and $\lambda = 10$ (green). The control with $\lambda = 100$ produces identical results to that with no delay at this scale.

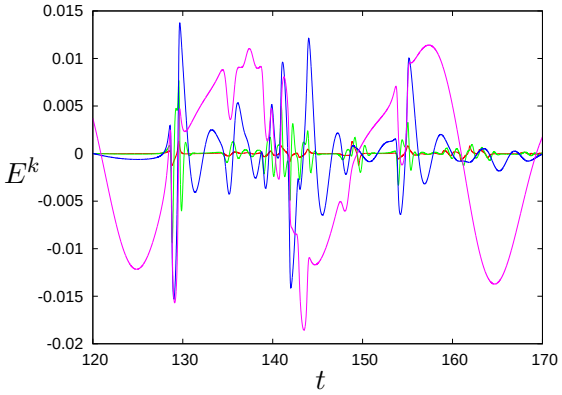


Figure 19. Error $E^k$ for controller (14)-(16) with $\mu_0 = 15$, $\Delta = 0$ and $\mu_1 = 100$ applied to case 6 with no delay (red), $\lambda = 1$ (green), $\lambda = 0.1$ (blue) and $\lambda = 0.01$ (magenta).

The norm values in Fig. 17 are for flow cases with a relatively small period of $T = 2.5$. As discussed previously, this represents flow near the base of the blade. Increasing the value of $T$ gives a more realistic representation of the turbine dynamics over most of the blade. Figures 18 and 19 illustrate the error signals when the two term controller is applied to case 6 (12 vortices, T=20) with $0.01 \leq \lambda \leq 100$, and Figure 20 the ratios of the error norms for cases 4-6. Again there is good attenuation with $\lambda = 10$ and $\lambda = 100$ (Fig. 18). However, in this case, significant attenuation is also achieved with $\lambda = 1$, as can be seen from Figure 20 and by comparing Figures 15 and 19. In particular, in all three cases the value of $\mathcal{L}_2$ is less than 3% of the value with no control, while, for cases 4 and 5, $\mathcal{L}_\infty$ is less than 1% of the uncontrolled value, and for case 6, it is approximately 20%. Also, as shown in Figure 20, there is a significant decrease in both measures of the error for all of cases 4-6 when $\lambda = 1$, in contrast to cases 1-3 (Figure 17). In strong contrast to cases 1-3, there is attenuation of the errors in cases 4-6 with $\lambda = 0.1$, in particular , in $\mathcal{L}_2$, but also in $\mathcal{L}_\infty$ for cases 4 and 5. This reflects the change in the period of the imposed oscillation in the flow as compared to the delay in the actuation with a fixed value of $\lambda$. With $\lambda = 0.01$ a different pattern emerges. Here there is a degree of damping (although less than with larger $\lambda$) for case 6, but an significant increase in the error norms for cases 4 and 5 (Figure 20). This is a result of the difference in the period of the imposed oscillation for cases 4 and 5 ($T = 10$) and for case 6 ($T = 20$). Specifically, for cases 4 and 5, the delay in the actuation leads to a situation where the actuation and imposed oscillation are out of phase (as compared to case 6). This is illustrated in Figure 21 which shows the velocity perturbation $(V_{0x} - 1)$ and control input $u^k$ for cases 5 and 6. There is a clear change in phase for the input relative to the imposed oscillation in the two cases. In contrast, with e.g.

$\lambda = 10$, when there is strong damping for both case 5 and case 6, the relative phase is the same for both cases, i.e. resembling that for case 6 with $\lambda = 0.01$ not case 5.

Since unit time in non-dimensional terms is the characteristic for a flow structure to be convected past the airfoil, it is not surprising that $\lambda$ needs to be 10 or greater in order to obtain the most effective damping of the fluctuations in the lift caused by disturbances such as vortices which are convected past the airfoil. As seen above, the value of $\lambda$ required to significantly effect the fluctuations due to the oscillatory nature of the free stream would depend on the period $T$. In general, our results show that $\lambda T \geq 10$ provides good attenuation of the oscillatory component of the lift.

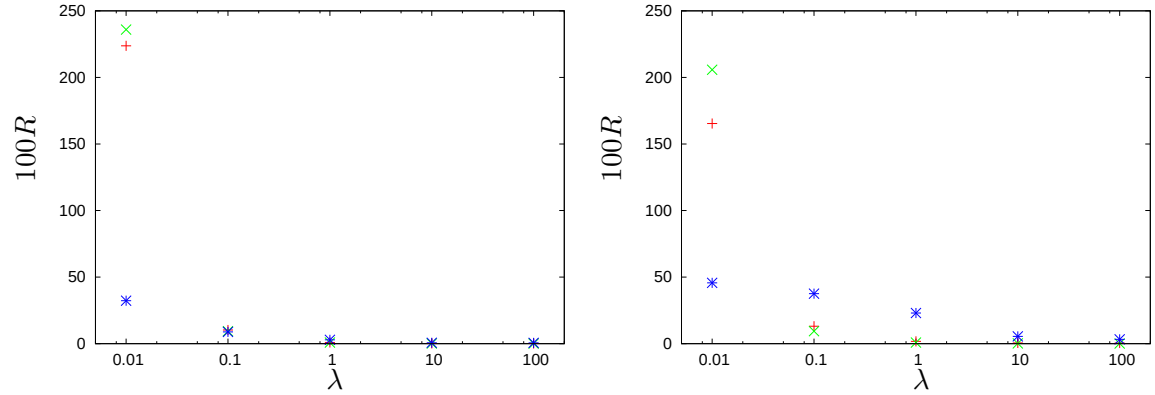


Figure 20. Error norms for controller (14-16) with $\mu_0 = 30$, $\mu_1 = 1$ and $\Delta = 0$ for different $\lambda$; left, $\mathcal{L}_2$ and right, $\mathcal{L}_\infty$. Case 4 (red), case 5 (green) and case 6 (blue). $R$ is the ratio of the norms against the values for no delay.

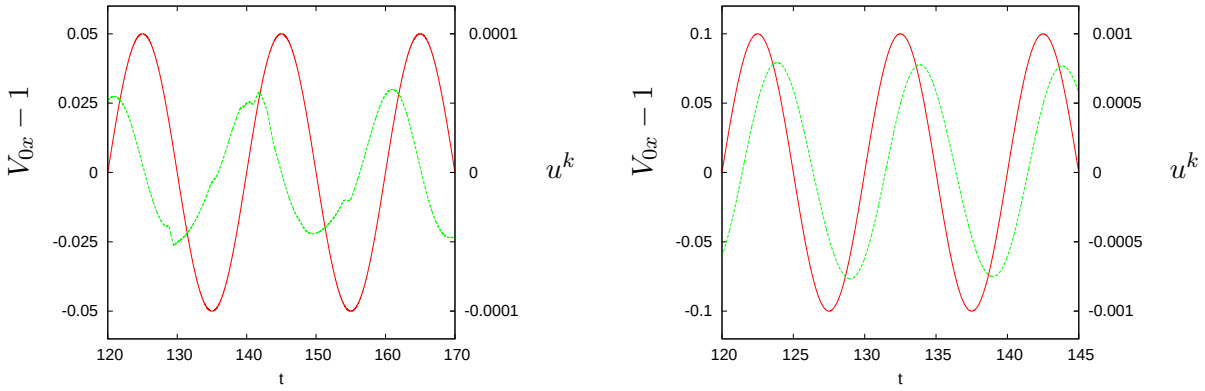


Figure 21. Free stream velocity oscillation (red) and control input (green) for case 5 (left) and case 6 (right).

In physical terms, taking $\lambda = 10/T$, the 90% response time of the actuation ($2.3/\lambda$ in non-dimensional terms) is approximately $t_c^*/5$, where $t_c^*$ is the rotation time of the turbine. A modern turbine of 100m or greater diameter will have a characteristic rotation time of 5s , giving a 90% response time of 1s, within the capabilities of, e.g., a trailing edge flap (see e.g. Castaignet et al. (2013)). However, the response time required to significantly damp out the effect of convective disturbances is much more demanding. Assuming the free stream velocity $V_\infty$ comes mainly from the rotation of the blade , $V_\infty \approx 2\pi R/t_c^*$ where $R$ is the radial distance from the axis of the airfoil section. Then, taking $\lambda = 10$, the 90% response time is approximately $t_c^* H/30R$. With a 5s rotation time, and a 1m chord blade 40m from the axis, this would require a 90% response time of around 0.004s. Closer to the hub, a slower response could be tolerated (e.g. around 0.03s for a 2.5m chord

blade at 10m from the axis), but still much more demanding than that required to damp the oscillatory component of the lift.

## 6. CONCLUSIONS

A simple but realistic CFD model has been applied to the problem of oscillatory flow past an airfoil with vortical disturbances in the flow, interacting non-linearly with the airfoil, and with trailing edge vorticity/circulation generation for actuation, as a model of a section of a smart wind turbine rotor blade. Discrete vortices are shed into the airfoil wake from the trailing edge every time step to model the Wagner effect. This model has then been used for a detailed initial investigation into the application of simple structure ILC in this area. The need to build a state-space representation of the dynamics is not required and the simple structure ILC laws can be designed by consideration of the system output. Two different measures were used to assess the ability of the method to damp the disturbances, a 2-norm (fatigue load) and an $\infty$-norm (extreme/peak load). In general, with control, the 2-norm was an order of magnitude or more lower than for the corresponding case with no control, while the $\infty$-norm was around one order of magnitude lower. Performance was maintained in extreme cases with strong disturbances in the flow. Similar flow cases in previous work (Tutty et al., 2013) used a model without capturing the wake dynamics. The current model, with wake effects included, shows similar norm ratios to the previous work, with acceptable performance over a wide range of behaviour. Additionally, actuator dynamics were modeled as a first-order lag on the control input. Actuator performance limits have been identified and the control scheme has been shown to demand an achievable actuator bandwidth specification to significantly damp the oscillatory component of the lift. However, damping the transients produced by disturbances convected past the airfoil would require a much faster response, approaching the kHz level towards the tip of a 100m diameter blade. Model based ILC design is also very well advanced and an obvious area for further research is to consider them for this application by constructing a state-space model representation of the dynamics from the CFD generated data. The control laws in this paper do, however, have simple hardware implementations whereas model based methods often require state estimation. Hence it is necessary to fully evaluate their effectiveness and the results in this paper provide a significant step in this direction.

ILC is one approach to control design in this application area. A closely related approach is repetitive control and there has been research on the application of this design to wind turbine problems, e.g., Houtzager et al. (2013). Once both approaches are sufficiently mature, an obvious area for future research is an in-depth comparative performance evaluation to aid the commissioning engineer.

## References

Johnson, S.J., van Dam, C.P. & Berg, D.E. (2008). *Active load control techniques for wind turbines*. Sandia National Laboratories, SAND2008-4809.

Rice, J. K. & Verhaegen, M. (2010). Robust and Distributed Control of a Smart Blade. *Wind Energy*, *13* (2-3), 103–116.

Andersen, P. B.,Henricksen, L., Gaunaa, M., Bak, C. & Buhl., T. (2010) Deformable Trailing Edge Flaps for Modern MegaWatt Wind Turbine Controllers Using Strain Gauges. *Wind Energy*, *13* (2-3), 93–206.

Lackner, M.A.& van Kuik, G.A.M. (2010). The performance of wind turbine smart rotor control approaches during extreme loads", *Journal of Solar Energy Engineering*, *132*, 011008.

Castaignet, D., Barlas, T., Buhl, T., Poulsen, N.K., Wedel-Heinen, J.J., Olesen, N.A., Bak, C. & Kim, T. (2013). Full-scale test of trailing edge flaps on a Vestas V27 wind turbine: active load reduction and system identification. *Wind Energy*, DOI:10.1002/we1589.

Johnston, S. J., Baker, J.P., van Dam, C.P. & Berg, D. (2010). An overview of active load control techniques for wind turbines with an emphasis on microtabs. *Wind Energy*, *13* (2-3), 239–253.

Chow, R. & van Dam, C.P. (2010). On the temporal response of devices. *Wind Energy*, *13* (2-3), 135–149.

Veers, P. S., Ashwill, T.D., Sutherland, H.J., Laird, D.L. & Lobitz, D.W. (2003). Trends in the design, manufacture and evaluation of wind turbine blades. *Wind Energy*, *6* (3), 245–259.

Bristow, D.A., Tharayil, M. & Alleyne, A.G. (2006). A survey of iterative learning control. *IEEE Control Systems Magazine*, *26*, 96–114.

Ahn, H.S., Chen, Y. & Moore, K.L. Iterative learning control: brief survey and categorization 1998–2004. *IEEE Transactions on Systems Man and Cybernetics Part C*, *37*, 1099–1121.

Laks, J., Pao, L. & Alleyne, A.G. (2011). Comparison of wind turbine operating transitions through the use of iterative learning control. *American Control Conference*, San Francisco, 4312–4319.

Tutty, O., Blackwell, M., Rogers, E. & Sandberg, R. Iterative learning control for improved aerodynamic load performance of wind turbines with smart rotors. *IEEE Transactions on Control Systems Technology*, DOI:10.1109/TCST.2013.2264322.

Dong, J. & Verhaegen, M. (2011). *Data driven fault detection and isolation of a wind turbine benchmark*, Proceedings of the 18th IFAC World Congress, 7086–7091.

Thomsen, S.J., Niemann, H. & Poulsen, N.J. Stochastic wind turbine control in multiblade coordinates. *Proc. American Control Conference*, 2777–2782.

Somers, D.M. (2005). *Design and Experimental Results for the S825 airfoil*, NREL Report, NREL/SR-500-36346.

Clarke, N.R. & Tutty, O.R. (1004). Construction and Validation of a discrete vortex method for the two-dimensional incompressible Navier-Stokes equations. *Computers & Fluids*, *23*, 51-783.

Anderson, J.D. (1985). *Fundamentals of Aerodynamics*, McGraw-Hill.

Batchelor, G.K. (1967). *An Introduction to Fluid Dynamics*, Cambridge University Press, 1967.

Cottet, G. H. & Koumoutsakos, P. D. (2008) *Vortex Methods: Theory and Practice*, Cambridge University Press.

Gaunaa, M. (2010). Unsteady two-dimensional potential-flow model for thin variable geometry airfoils, *Wind Energy*, *13*, 167–19.

XFOIL, Available from http://web.mit.edu/drela/Public/web/xfoil/, 1985.

Houtzager, I., van Wingerden, J.-W. & Verhaegen, M. (2013). Rejection of periodic wind disturbances on a smart rotor test section using lifted repetitive control. *IEEE Transactions on Control Systems Technology*, *21* (2), 347–358.